analytical chemistry

Article

Cite This: Anal. Chem. 2018, 90, 8785−8792

pubs.acs.org/ac

Highly Sensitive Fluorescence Imaging of Zn^{2+} and Cu^{2+} in Living Cells with Signal Amplification Based on Functional DNA Self-Assembly

Haibin Si, Renjie Sheng, Qingling Li, Jie Feng, Lu Li,* and Bo Tang*

College of Chemistry, Chemical Engineering and Materials Science, Key Laboratory of Molecular and Nano Probes, Ministry of Education, Collaborative Innovation Center of Functionalized Probes for Chemical Imaging, Institute of Molecular and Nano Science, Shandong Normal University, Jinan, 250014 Shandong, People's Republic of China

Supporting Information

ABSTRACT: Intracellular trace Zn^{2+} and Cu^{2+} play important roles in the regulation of cell function. Considering the limitations of existing metal ion detection methods regarding sensitivity and applicability to living cells, an amplification strategy based on functional DNA self-assembly under DNAzyme catalysis to improve the sensitivity of intracellular Zn^{2+} and Cu^{2+} imaging is reported. In this process, metal ions as cofactor can activate the catalysis of DNAzyme to shear substrate chains, and each broken substrate chain can initiate consecutive hybridizations of hairpin probes (Hx) labeled with fluorophore, which can reflect the information on a single metal ion with multiple fluorophores. The detection limit can reach nearly 80 pM and high-sensitivity fluorescence imaging of intracellular Zn^{2+} and Cu^{2+} can be achieved. The results are important for research on cell function regulation associated with trace Zn^{2+} and Cu^{2+}. This approach is also a new way to improve the sensitivity of other trace metal ion imaging.

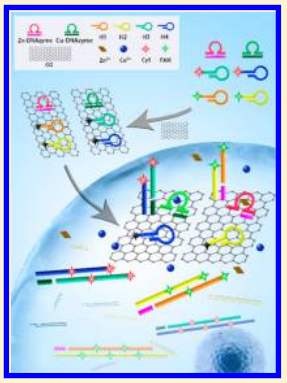

Zn^{2+} and Cu^{2+} are vital (both useful and cytotoxic) trace metal ions in living cells. As necessary heavy metal elements in the human body, Zn^{2+} and Cu^{2+} play essential roles in many physiological and pathological processes, although both excess and lack of Zn^{2+} and Cu^{2+} can lead to abnormal cell function and disease. Research has shown that moderate amounts of Zn^{2+} play an active role in gene transcription and neurotransmission[1−3] and that the element is also an important component of multiple enzymes and DNA-binding proteins.[3−5] Nevertheless, abnormal Zn^{2+} concentrations are closely related to various neurological diseases, such as Alzheimer's and Parkinson's.[6] As another important trace metal ion, appropriate amounts of Cu^{2+} have important functions in biological processes such as enzyme regulation, metabolism, and immunity, but excess Cu^{2+} can lead to liver or kidney damage and several neurodegenerative diseases.[7−11] In addition, some studies have indicated that intracellular Zn^{2+} and Cu^{2+}, which extensively regulate biological function, are interactive with and complementary to each other.[12,13] Therefore, the detection of intracellular Zn^{2+} and Cu^{2+} has a very important significance for understanding the relevant cell function regulation and the occurrence of disease.

Traditionally, the main methods for detecting metal elements are atomic absorption spectrometry (AAS),[14−17] inductively coupled plasma atomic emission spectrometry (ICP-AES),[18−21] inductively coupled plasma mass spectrometry (ICP-MS),[22−24] and so on. Complex chemical treatments of samples are necessary for the above methods, which are not suitable for the in situ detection of the distribution and concentration of Zn^{2+} and Cu^{2+} in living cells. To overcome the shortcomings of these traditional methods, fluorescence methods have gained added attention because of their simplicity, rapid response, and noninvasive characteristics. For intracellular Zn^{2+} and Cu^{2+} detection and imaging, many organic fluorescent probes have been developed in succession. However, these fluorescent probes usually react with Zn^{2+} and Cu^{2+} at a ratio of 1:1, the detection limit is generally at the level of 10 nM.[25−31] Because of the ultralow concentrations of free Zn^{2+} and Cu^{2+} in cells,[32,33] improving the sensitivity of fluorescent methods is still urgent and important. Considering the complexity of designing responsive organic fluorescent probes, it is very difficult to design a signal amplification strategy based on organic fluorescent probes. Therefore, developing new fluorescence methods to improve the sensitivity of intracellular Zn^{2+} and Cu^{2+} detection is necessary. Owing to the great progress in biotechnology, DNAzyme sensors with high selectivity to metal ions have received increased attention in recent years.[34−39] However, research using DNAzymes for in situ monitoring of intracellular metal ion is still relatively rare. In 2013, Lu group pioneered the use of DNAzymes to achieve UO^{2+} fluorescence detection in living cells.[40] Subsequently, the group conducted some studies on the use of DNAzymes for intracellular metal ion imaging.[41−43] In addition, because DNAzymes have excellent adaptability to numerous fluorescent groups, they can be labeled with various

Received: December 18, 2017
Accepted: July 5, 2018
Published: July 5, 2018

DOI: 10.1021/acs.analchem.7b05268
Anal. Chem. 2018, 90, 8785−8792

organic fluorescent dyes to achieve the simultaneous detection and imaging of a variety of metal ions.[44] As the ratio of fluorescence labels to the metal ions is 1:1 in the above imaging methods, the development of signal amplification strategies to improve the detection sensitivity in living cells is an urgent need. Although the Lu group has just reported the real-time imaging of endogenous sodium ions using a catalytic hairpin assembly (CHA) reaction,[45] for trace metal ions such as Zn^{2+} and Cu^{2+} with lower levels of cells, developing new signal amplification strategies to improve the imaging sensitivity is still important. Furthermore, the application of signal amplification strategies in simultaneous distinction of multiple metal ions is even more challenging.

The hybridization chain reaction (HCR), which was first proposed by Dirk and Pierce,[46] is an amplification method where DNA self-assembly is triggered by initiator DNA under mild conditions. Its amplification process is an ideal means to achieve high-sensitivity detection of the target with low concentration, which has been widely used for detecting various biological targets.[47−51] Inspired by the above information, we combined the recognition function of DNAzymes and the amplification ability of the HCR to develop a strategy capable of achieving signal amplification for the simultaneous detection of intracellular Zn^{2+} and Cu^{2+}. Considering the application of this signal amplification strategy in complex cell environments, a platform that can carry and transport biomolecules is necessary, as such a platform can support combinations of biomolecules and achieve a variety of signal transitions. Recently, various nanostructures, such as graphene oxide (GO),[52] quantum dots,[53−55] carbon nanotubes,[56] gold nanoparticles,[57−60] and ferromagnetic nanoparticles,[61] have been used as sensor substrates. As a nonmetallic material, graphene has been used increasingly for its lack of metal toxicity, superior biocompatibility, and facile surface modification.[62,63] Its unique planar adsorption capacity allows the sensor to be assembled without using nonchemical modification conditions, thereby reducing the complexity of the preparation method. In addition, as an energy receptor, GO is an ideal sensor base material that can simultaneously serve as a fluorescence quencher.

In this work, we report a signal amplification strategy for the high-sensitivity detection and simultaneous in situ imaging of Zn^{2+} and Cu^{2+} in living cells. The strategy is achieved by a sensor consisting of a DNAzyme, a hairpin probe (Hx), and biocompatible GO as intracellular transport carrier. In the presence of metal ions, the sensor enables the imaging of these metal ions through signal amplification based on DNA self-assembly under DNAzyme catalysis. This is the first time using a signal amplification strategy for simultaneous imaging of multiple metal ions in living cells. The detection limits of the method can reach 100 pM and 80 pM respectively, which is nearly 2 orders of magnitude higher than the sensitivity of the existing organic fluorescent probes.

EXPERIMENTAL SECTION

Chemicals and Apparatus. Oligonucleotides were synthesized and purified by high-performance liquid chromatography (HPLC) by Sangon Biotech Co., Ltd. (Shanghai, China). Their sequences are listed in Table S1. GO was purchased from XF Nano, Inc. (Nanjing, China); 3-(4,5-dimethyl-thiazol-2-yl)-2,5-diphenyl-tetrazolium bromide (MTT) was purchased from Sigma Chemical Company (St. Louis, U.S.A.); KCl, NaCl, $Cu(CH_3COO)_2{\cdot}H_2O$, $Mn(CH_3COO)_2{\cdot}4H_2O$, $Co(CH_3COO)_2{\cdot}4H_2O$, $Cd(NO_3)_2{\cdot}6H_2O$, $Zn(CH_3COO)_2{\cdot}2H_2O$, $CaCl_2$, $FeCl_3$, $Ni(CH_3COO)_2{\cdot}4H_2O$, $Pb^{2+}(CH_3COO)_2$, and PDCA were purchased from China National Pharmaceutical Group Corporation (Shanghai, China). Cell culture products, unless mentioned otherwise, were purchased from Gibco. The MCF-7 cells was purchased from KeyGEN biotechnology Company (Nanjing, China). All the chemicals were of analytical grade and used without further purification. Deionized water was obtained through a Sartorius Arium 611 VF system (Sartorius AG, Germany) with a resistivity of 18.2 MΩ·cm. All pH measurements were performed with a pH-3c digital pH-meter (Shanghai LeiCi Device Works, Shanghai, China) with a combined glass-calomel electrode. Centrifugation was performed with a Sigma 3K15 refrigerated centrifuge. The fluorescent spectra were measured using a Cary Eclipse fluorescence spectrophotometer (Varian, California). For the MTT assay, absorbance was measured in a microplate reader (RT 6000, Rayto, U.S.A.). Confocal fluorescence imaging studies were performed with a TCS SP5 CLSM (Leica Co., Ltd. Germany) with an objective lens (×40).

Preparation of DNAzyme. To form the Cu^{2+}-dependent DNAzymes, a mixture of 2 μM Cu-substrate and 2 μM Cu-Enzyme was warmed to 95 °C for 5 min in a water bath and then allowed to cool to room temperature for 1 h. The resultant DNAzymes were stored in a 4 °C dark room. The preparation processing of the Zn^{2+}-dependent DNAzyme was the same as above.

Preparation of Hairpin DNA Probes. The FAM-labeled hairpin DNA probes (2.5 μM FAM-H1 and 2.5 μM FAM-H2) were separately heated at 95 °C for 5 min in a water bath and then allowed to cool to room temperature for 1 h to make the probe perfectly fold into a hairpin structure. The resultant hairpin DNA probes were stored in a 4 °C dark room before use. The preparation processing of the FAM-H3, FAM-H4, Cy5-H3, and Cy5-H4 were the same as above.

Fluorescence Measurements. Fluorescence measurements were conducted on a Cary Eclipse fluorescence spectrophotometer. In a typical experiment, 350 μL of buffer (50 mM PBS, 50 mM NaCl, pH 7.4), 10 μL of H1, 10 μL of H2, 20 μL of DNAzyme, and 100 μL of graphene solution (500 μg/mL) were sequentially added into a microcentrifuge tube. After a 10 min reaction, 10 μL of Cu^{2+}/Zn^{2+} stock solution was added to the mixture. After reacting at 37 °C for 60 min, the fluorescence of FAM was collected between 500 and 600 nm using an excitation wavelength of 488 nm, and the fluorescence of Cy5 was collected between 645 and 750 nm using an excitation wavelength of 633 nm.

Gel Electrophoresis Analysis. The 2% agarose gels contained 2 μL of Gelred per 30 mL of gel volume, and were prepared using TBE buffer (0.5×). A volume of 6 μL of different reaction products with loading buffer (1×) was added to each lane. Agarose gels were run at 110 V for 40 min inTBE buffer (0.5×) and visualized under UV light.

Selectivity Experiment. The Zn^{2+} and Cu^{2+} stock solutions were added into the mixed solution to afford a final concentration of 5 μM. For the other metal ions, the concentrations were 1.0 mM for K^+ and Ca^{2+}; 25 μM for Fe^{3+}, Co^{2+}, Ni^{2+}, Mn^{2+}, and Cd^{2+}; and 25 μM for Pb^{2+} with 50 μM PDCA. The measuring process was the same as above.

Cell Culture. MCF-7 cells were cultured in 1640 medium supplemented with 10% fetal bovine serum, 100 U/mL

DOI: 10.1021/acs.analchem.7b05268
Anal. Chem. 2018, 90, 8785−8792

penicillin, and 100 μg/mL streptomycin and incubated at 37 °C in a humidified atmosphere of 5% CO_2 and 95% air.

MTT Assay. To investigate the cytotoxicity of the GO/probe, an MTT assay was conducted. MCF-7 cells (1×10^6 cells/well) were dispersed within replicate 96-well microtiter plates to a total volume of 200 μL $well^{-1}$. The plates were maintained at 37 °C in a 5% CO_2/95% air incubator for 24 h. After the original medium was removed, the MCF-7 cells were incubated with GO (0, 3.125, 6.25, 12.5, 25, 50, 100, or 200 μg/mL) or GO/probe (the final GO concentrations were 0, 3.125, 6.25, 12.5, 25, 50, 100, and 200 μg/mL; the probe consisted of 50 nM H1, 50 nM H2, and 40 nM DNAzyme) for 12 h. Then, 100 μL of MTT solution (0.5 mg mL^{-1} in PBS) was added to each well. After 4 h, the remaining MTT solution was removed, and 150 μL of DMSO was added to each well to dissolve the formazan crystals. The absorbance was measured at 490 nm with an RT 6000 microplate reader.

Imaging of Cu^{2+}/Zn^{2+} in Living Cells. MCF-7 cells were cultured in 1640 medium for 24 h. Next, the cells were incubated with Zn^{2+} and Cu^{2+} solution at 37 °C in 5% CO_2 for 60 min and then were washed three times with fresh 1640 medium. Finally, the mixture of GO (100 μg/mL), H1 (50 nM), H2 (50 nM), and DNAzyme (40 nM) was delivered into MCF-7 cells in fresh 1640 culture medium for 12 h, and then the cells were washed three times with PBS. Fluorescence images were acquired on a CLSM with different laser transmitters. Zn^{2+} was determined using the fluorescence of FAM in the green channel with 488 nm excitation, whereas Cu^{2+} was determined using the fluorescence of Cy5 in the red channel with 633 nm excitation.

RESULTS AND DISCUSSION

Imaging Principle of the Sensor for Zn^{2+} and Cu^{2+}. The imaging principle is shown in Scheme 1. The intracellular Zn^{2+} and Cu^{2+} sensors consist of the Zn/Cu-DNAzyme probes and fluorophore-labeled hairpin probes Hx (H1, H2, H3, and H4) loaded onto GO. The DNAzyme probe is a double-stranded DNA comprising a DNAzyme and a DNA substrate chain with a partial single-stranded DNA loop on DNAzyme. DNAzymes are sequences of DNA that have the ability to catalyze many chemical and biological reactions. Most of these reactions require special metal ions as cofactors. When the metal ion cofactor is bound at the single-stranded loop, it activates the catalysis of DNAzyme on the cleavage of the phosphodiester backbone at a ribonucleotide site on substrate chain.[64−67] The hairpin probe H1 and H2 are labeled with a fluorophore FAM for fluorescence imaging of Zn^{2+} while hairpin probe H3 and H4 are labeled with a fluorophore Cy5 for fluorescence imaging of Cu^{2+}. GO, the sensor substrate, is an atomically thin carbon material with good water solubility and biocompatibility. In the assembly process of the sensor, the partial single-stranded DNA loop structure of the Zn/Cu-DNAzyme and the hairpin probe Hx interact with GO through π−π stacking,[68] which allows these molecules to be assembled on the GO substrate. Initially, GO serves as an energy receptor and quenches the fluorescence of the fluorophores labeled on the hairpin probe through the fluorescence resonance energy transfer effect. When the graphene-based sensors entered cells through endocytosis, the substrate chain could be sheared under DNAzyme catalysis in the presence of free metal ions in the cells. The HCR is then triggered by the released DNA fragment. In the case of Zn^{2+} detection, the DNA fragments were released under the catalysis of the Zn-DNAzyme in the presence of Zn^{2+}. The released DNA fragments can hybridize with part of hairpin H1 labeled with FAM, thereby opening the hairpin structure of H1. The opened H1 are complementary to the partial structure of H2, allowing hairpin probes H2 to be opened. Long double-stranded DNA can be obtained by the HCRs of H1 and H2. As the interactions between GO and the double-stranded DNA are reduced, the quenched fluorescence is recovered.[69,70] In this process, Zn^{2+} can trigger the cleavage of Zn-substrate chains, and each broken substrate chain can initiate multiple hybridizations of H1 and H2, which can reflect the information on single Zn^{2+} with multiple fluorophores labeled on H1 and H2. Intracellular Zn^{2+} can be imaged by the amplified fluorescence produced from functional DNA self-assembly under the catalysis of the DNAzyme. Another pair of hairpin probes labeled with Cy5, H3 and H4, were designed in the same way. In the presence of Cu^{2+}, the DNA fragments are released under the catalysis of the Cu-DNAzyme. The released DNA fragments are complementary to the Cy5-labeled H3, leading to the HCRs of H4 and H3. The intracellular Cu^{2+} can also be amplified and imaged by the fluorescence signal produced from HCRs.

Scheme 1. Design of a Signal Amplification Sensor for the Highly Sensitive Fluorescence Imaging of Zn^{2+} and Cu^{2+} in Living Cells

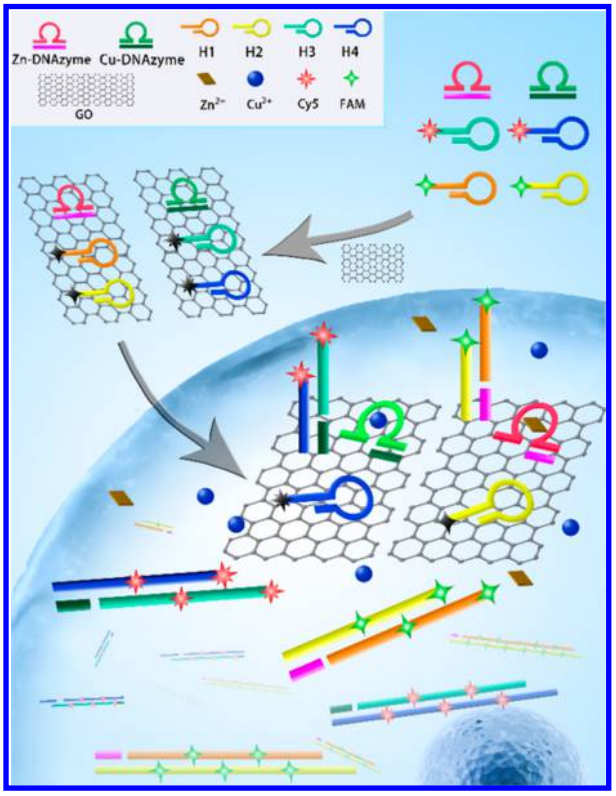

Fluorescence Detection of Zn^{2+} and Cu^{2+} in Solution by the Zn^{2+} and Cu^{2+} Sensors. To confirm the response of sensors to Zn^{2+} and Cu^{2+}, we first perform the fluorescence detection of Zn^{2+} and Cu^{2+} in solution (0.05 M PBS, 0.05 M NaCl, pH = 7.4). The Hx were all labeled with FAM, and the fluorescence signal was excited with a 488 nm laser. Figure 1 shows the fluorescence spectra of the sensors in different systems. The fluorescence intensity of Zn^{2+}-DNAzyme/H1 + H2 supported on GO (GO/DNAzyme/H1 + H2, blue curve) is much weaker than that of Zn^{2+}-DNAzyme/H1 + H2 not supported on GO (black curve). This result indicates that GO

DOI: 10.1021/acs.analchem.7b05268
Anal. Chem. 2018, 90, 8785−8792

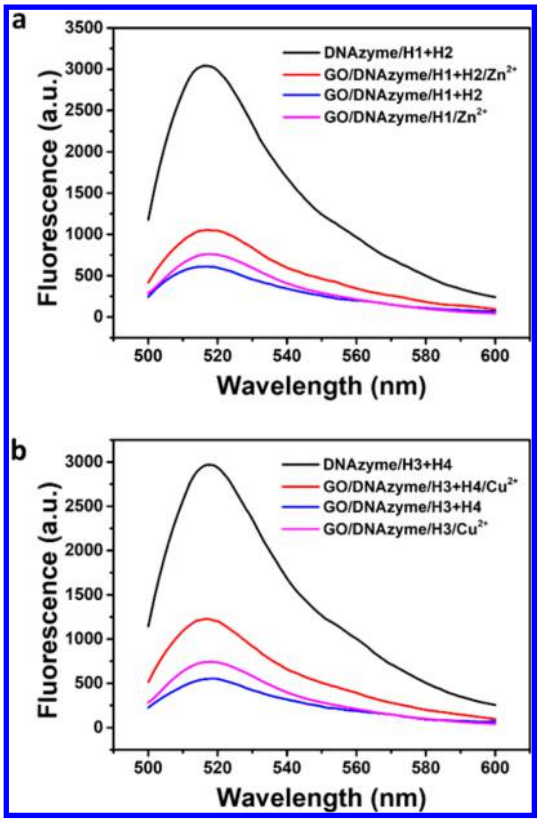

Figure 1. Fluorescence spectra of the sensor in solution. (a) Fluorescence spectra of DNAzyme/H1 + H2 (balck curve), GO/DNAzyme/H1 + H2 in the absence (blue curve) and presence (red curve) of Zn^{2+}, and GO/DNAzyme/H1 in the presence of Zn^{2+} (purple curve). (b) Fluorescence spectra of DNAzyme/H3 + H4 (black curve) and GO/DNAzyme/H3 + H4 in the absence (blue curve) and presence (red curve) of Cu^{2+}. GO/DNAzyme/H3 in the presence (purple curve) of Cu^{2+}. The concentration of both Zn^{2+} and Cu^{2+} was 5 μM. The curves were measured with 488 nm excitation.

has a very strong quenching effect on the fluorophores. When Zn^{2+} (5 μM) was added to the solution, the fluorescence intensity at 518 nm was significantly increased (red curve), indicating that, in the presence of Zn^{2+}, the DNA substrate was cleaved under the catalysis of the DNAzyme and the released DNA fragments succeeded in triggering the HCRs. In order to verify the signal amplification effect of HCR, the fluorescence response of Zn^{2+}-DNAzyme/H1 supported on GO (GO/DNAzyme/H1) for Zn^{2+} were investigated. The obtained fluorescence spectra of GO/DNAzyme/H1 complex (purple curve) show that individual H1-loaded sensor also produce Zn^{2+}-specific fluorescence responses. However, the fluorescence signal is much weaker than that of the GO/DNAzyme/H1 + H2 sensor. This shows that only the coexistence of H1 and H2 can perform the HCR reaction, thereby amplifying the Zn^{2+} signal. Similarly, the increased fluorescence signal (Figure 1b) can be observed when using GO/Cu^{2+}-DNAzyme/FAM-H3/FAM-H4 sensor in the presence of Cu^{2+}, thereby confirming the feasibility of the scheme for the detection of Cu^{2+}.

Optimization of the Sensor. The concentration ratio of GO to the nucleotide probes will affect the quenching effect of GO on the fluorophore labeled on the hairpin probe. To investigate the optimum concentration ratio of GO to the DNAzymes and hairpin probes, we used 0, 20, 40, 60, 80, 100, 120, and 150 μg/mL of graphene with 0.08 μM DNAzymes and 0.05 μM hairpin probes. The fluorescence intensity was measured in the presence and absence of metal ions. As shown in Figure S1a, the blue line obtained in the absence of Zn^{2+} shows the changes in the fluorescence intensity of the fluorophore with different concentrations of GO, whereas the black line obtained in the presence of Zn^{2+} exhibits the fluorescence recovery caused by Zn^{2+}. In general, the signal-to-noise ratio depends on the difference in the values of fluorescence intensity (defined as the relative fluorescence intensity) in the presence and absence of metal ions. Clearly, the S/N is greatest when the concentration of GO reaches 100 μg/mL. The results obtained in Figure S1b show that the optimized concentration is also applicable to the detection of Cu^{2+}.

In this metal ion sensor, the DNAzymes and hairpin probes Hx were adsorbed onto GO by $\pi-\pi$ stacking interaction between the nucleotide bases in the single-stranded DNA loop structure and GO. This adsorption is a process that gradually reaches equilibrium over time. An optimized adsorption time can not only increase the adsorption capacity of the probe but also avoid an overly long detection time. The fluorescence quenching of the hairpin probe by GO can reflect the adsorption of the DNAzyme and hairpin probes onto GO. Therefore, we monitored the fluorescence intensity changes in the system after mixing GO, the DNAzyme and the hairpin probes for different times. The results of the experiment when the GO concentration is 100 μg/mL are shown in Figure S2. In the first 0−10 min, the fluorescence intensity of the fluorophore decreases with the prolongation of the mixing time. When the reaction time is greater than 10 min, the fluorescence intensity no longer changes. This phenomenon indicates that 0.08 μM DNAzyme and 0.05 μM hairpin probe can achieve an adsorption equilibrium with 100 μg/mL GO within 10 min and that the GO has a good quenching effect on the fluorophores labeled on the hairpin probes. The mixing time was finally set to 10 min.

Characterization of the Performance of the Sensors. The ability of the system to quantify Zn^{2+} and Cu^{2+} was investigated. After 10 min of mixing the DNAzyme (0.08 μM), hairpin probes H1 and H2 (0.05 μM), and GO (100 μg/mL), different concentrations of Zn^{2+} were added to the system to measure the fluorescence intensity. Similarly, the fluorescence intensity of the probe with different concentrations of Cu^{2+} was also detected. The results are shown in Figure 2. Figure 2a,c presents the fluorescent spectra of the constructed sensors after reacting with Zn^{2+} and Cu^{2+} at different concentrations (0−200 nM). Figure 2b and d are the curves of the obtained fluorescence intensity vs the concentration of Zn^{2+} and Cu^{2+}. The fluorescence intensity is related to the concentration of Zn^{2+} and Cu^{2+}, with a good linear range from 0.25 to 2 nM and from 0.1 to 5 nM for the target Zn^{2+} and Cu^{2+}, respectively. The correlation linear equations for Zn^{2+} and Cu^{2+} are $y = 37.06x + 615.98$ and $y = 43.63x + 621.49$, respectively, with coefficients R1 = 0.9923 and R2 = 0.9904. Based on 3σ/slope, the detection limits of the sensor to the Zn^{2+} and Cu^{2+} were 0.1 and 0.08 nM, respectively. The detection limits were reduced by 4.7 and 5.6 times compared to those obtained from Zn^{2+} and Cu^{2+} detection without signal amplification in our previous work.[44] In addition, compared with organic fluorescent probes for detection of Zn^{2+} and Cu^{2+}, the sensitivity also has a greater advantage (Table S2). The

DOI: 10.1021/acs.analchem.7b05268
Anal. Chem. 2018, 90, 8785−8792

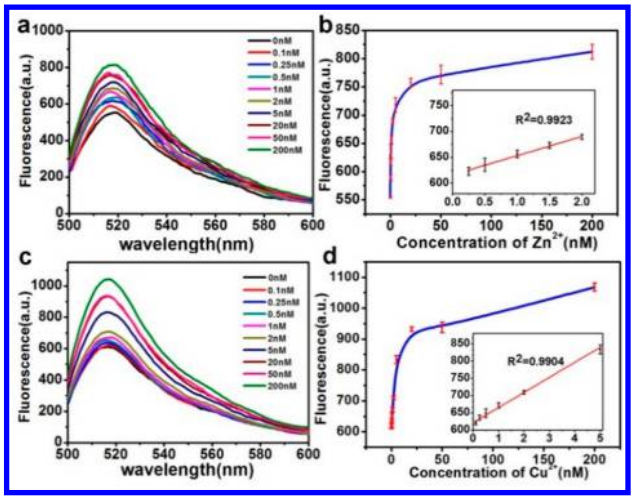

Figure 2. Fluorescence spectra of the probe in the presence of various concentrations of Zn^{2+} (a, b) and Cu^{2+} (c, d) (0, 0.10, 0.25, 0.50, 1.00, 2.00, 5.00, 20.00, 50.00, and 200.00 nM) measured with 488 nm excitation. Inset: calibration curves for the fluorescence intensity vs the corresponding target concentrations. The curves for Zn^{2+} and Cu^{2+} were both measured with 488 nm excitation. Error bars were estimated from three replicate measurements.

above results show that the developed method can detect Zn^{2+} and Cu^{2+} with high sensitivity.

To evaluate the selectivity of this method for the detection of the targets Zn^{2+} and Cu^{2+}, other different metal ions were also detected, such as Mn^{2+}, Cd^{2+}, Mg^{2+}, Co^{2+}, Fe^{3+}, Ca^{2+}, K^{+}, Ni^{2+}, and Pb^{2+}. The interference of Pb^{2+} can be eliminated by adding 2,6-pyridinedicarboxylic acid (PDCA), which can form a complex with Pb^{2+}.[71] As shown in Figure S3, the fluorescence intensity corresponding to lower concentration of Zn^{2+} and Cu^{2+} is much higher than that of other metal ions, even when they have higher concentration. Therefore, the method proposed in this paper has high specificity for Zn^{2+} and Cu^{2+} and can detect Zn^{2+} and Cu^{2+} in a complex biological system. Besides, the results also show that the method can detect Zn^{2+} in the presence of Cu^{2+} and Cu^{2+} do not interfere with Zn^{2+} detection, and vice versa.

In addition, the reaction kinetics of this method were evaluated. We measured the fluorescence intensity of the probe with Zn^{2+} and Cu^{2+} (both at 20 nM) at different times. The experiment results are shown in Figure S4. The intensity of the obtained fluorescence increased with the reaction time. When the reaction time reached 60 min, the fluorescence intensity no longer changed with time. The reaction time for Zn^{2+} was consistent with that for Cu^{2+}, which indicated the possibility that the two types of metal ions could be imaged simultaneously in cells. Further, we applied gel electrophoresis to perform the kinetic verification of the reaction and evaluate the amplification efficiency. In a typical experiment, the Zn^{2+} was added into the mixture solution containing H1, H2, and DNAzymes. After different reaction times, the products were analyzed. The result (Figure S5) shows that as reaction time was prolonged, long-chain products gradually increased, which has a similar trend with the reaction kinetics data from fluorescence test. When the reaction time was set to 1 h, the HCR products have a wider distribution of base number and most of the products have more than 500 bp, which illustrate the high amplification efficiency of this method.

To verify that the sensors are stable in a complex cell environment, we tested the stability of sensor with different pH and ionic strength. Since the sensors are endocytosed by the endosomes and eventually enter the cytoplasm, whereas the pH in endosomes is from 5 to 6.5 and the pH in cytoplasm is between 7.2 and 7.4, we tested the stability of the sensors in the pH range from 5 to 8. The Cy5-H3 and Cy5-H4 were adsorbed on GO and then incubated in PBS with different pH, followed by fluorescence detection. The results in Figure S6a show there is no significant changes in the fluorescence intensity of the sensors quenched by GO under the above pH range. This illustrates that our noncovalently assembled sensors have good stability at the above pH range. For ionic strength interference, we tested the stability of the sensors among 0.8× to 1.6× PBS with different ionic strength. As shown in Figure S6b, the quenching effect of GO on the sensors did not change significantly, demonstrating the stability of the sensor at above ionic strengths. It is well-known that DNAzyme is suspected to be cleaved by nuclease in cells, so we verified the stability of the DNAzyme and the DNAzyme loaded on GO in the presence of nuclease, and the reaction products were tested by gel electrophoresis. It can be seen from the gel electrophoretogram (Figure S7) that the DNAzyme alone was not stable in the presence of nucleases, while the DNAzyme loaded on GO showed a better stability. This may be due to the steric hindrance of GO limited the nuclease cleavage of nucleic acid sensors.[72−74]

Low cytotoxicity is a critical prerequisite for the application of sensors in living cells. MTT assays on human breast cancer cells (MCF-7) were performed to assess the cytotoxicity of GO and GO loaded with the probes. The absorption of MTT at 490 nm reflects the degree of cell activity. Cell viability can be expressed as the ratio of the absorbance of cells incubated with GO or GO loaded with the probes to the absorbance of untreated cells. The MTT testing results are illustrated in Figure S8. The activity of MCF-7 cells was not significantly affected by GO or GO conjugated with the probes at a concentration of less than 100 μg/mL up to 12 h, and the viability of the MCF-7 cells was confirmed.

Application of the Sensors in Imaging of Cellular Zn^{2+} and Cu^{2+}. To test the application of this method in a complex cellular environment, MCF-7 cells were chosen as a biological model for cell uptake and metal ions imaging. The cell experiments on Zn^{2+} and Cu^{2+} were first conducted separately. In the case of the Zn^{2+} imaging, MCF-7 cells were first incubated with different concentration Zn^{2+} solution for 1 h and then incubated with the GO/DNAzyme/H1 complex or GO/DNAzyme/H1 + H2 sensors, followed by fluorescence imaging. The results are shown in Figure 3. Without extra Zn^{2+} addition, MCF-7 cells have no cellular background fluorescence under our imaging conditions (Figure 3a). The images of MCF-7 cells incubated with GO/DNAzyme/H1 complex and GO/DNAzyme/H1 + H2 sensors also do not show significant fluorescence (Figure 3b,c), suggesting that rare desorption of H1 and H2 from GO, and the GO still had a very good quenching effect on the fluorophores labeled on the hairpin probes in the cells. So, we can conclude that the nonspecific adsorption between GO and nucleic acids/proteins in cytoplasm has no obvious effect on the sensor. After MCF-7 cells were first incubated with 5 μM Zn^{2+} solution then incubated with GO/DNAzyme/H1 + H2 sensors, a significant green fluorescence was observed in the confocal image (Figure 3f). A weak fluorescence was also observed when the Zn^{2+}-

DOI: 10.1021/acs.analchem.7b05268
Anal. Chem. 2018, 90, 8785−8792

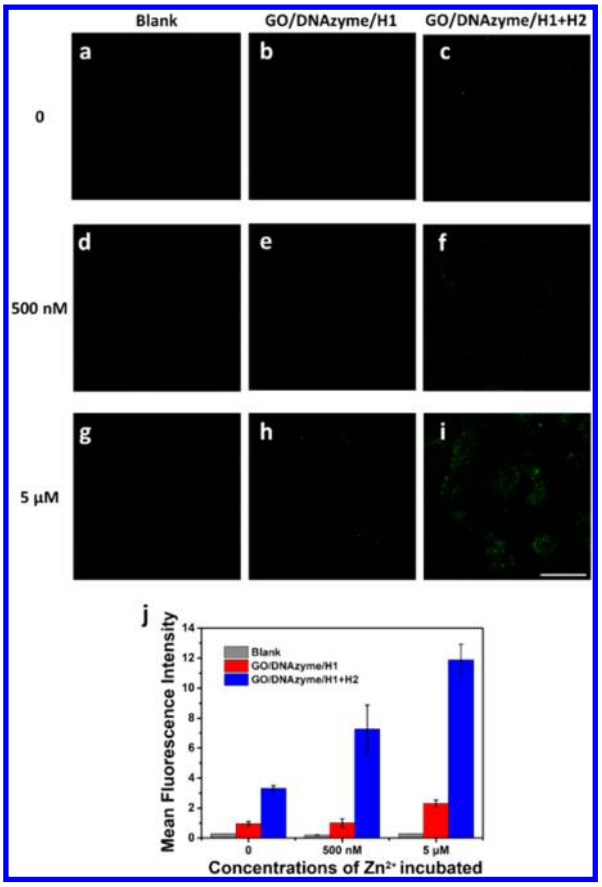

Figure 3. Fluorescence images (a–i) and quantitative analysis (j) of Zn^{2+} in MCF-7 cells using GO/DNAzyme/H1 + H2 sensors and GO/DNAzyme/H1 complex. Blank represents for cells without any sensors or complex added. The MCF-7 cells were incubated with Zn^{2+} solution of different concentrations (a–c, 0 nM; d–f, 500 nM; g, h, 5 μM). Scale bar is 50 μm.

added MCF-7 cells were incubated with the GO/DNAzyme/H1 complex (Figure 3e). These results indicates that both the GO/DNAzyme/H1 + H2 sensors and GO/DNAzyme/H1 complex can enter the MCF-7 cells and have fluorescence response to the intracellular Zn^{2+}. The more significant fluorescence from GO/DNAzyme/H1 + H2 sensors indicates that after the specifical DNAzyme recognization of Zn^{2+} and the effective enzyme catalysis, the released DNA fragments from cleavage of the substrate could induce the HCR in the present of H1 and H2 and then fluorescence cumulation. The weak fluorescence from GO/DNAzyme/H1 complex may come from the recovery of the fluorescence of H1 upon the hybridization of H1 and the DNA fragments. The results further demonstrates that the GO/DNAzyme/H1 + H2 sensors have signal amplification effect on Zn^{2+} in cells through the HCR. In order to further demonstrate the amplification effect of HCR on metal ions. We performed the intracellular Zn^{2+} imaging with GO/DNAzyme/H1 + H2 sensors and GO/DNAzyme/H1 complex respectively, after incubation with Zn^{2+} solution at lower concentration (500 nM). Under this condition, intracellular Zn^{2+} could not be effectively presented by GO/DNAzyme/H1 complex (Figure 3h), while the fluorescence can be observed by the GO/DNAzyme/H1 + H2 sensors (Figure 3i). Quantitative comparison has also been performed to illustrate the amplification efficiency of GO/DNAzyme/H1 + H2 sensors based on the average fluorescence intensity analysis of the cells in above images, the data are shown in Figure 3j. Similar results have also been obtained from the intracellular Cu^{2+} detection based on GO/DNAzyme/H3 + H4 sensors and GO/DNAzyme/H3 complex (Figure 4).

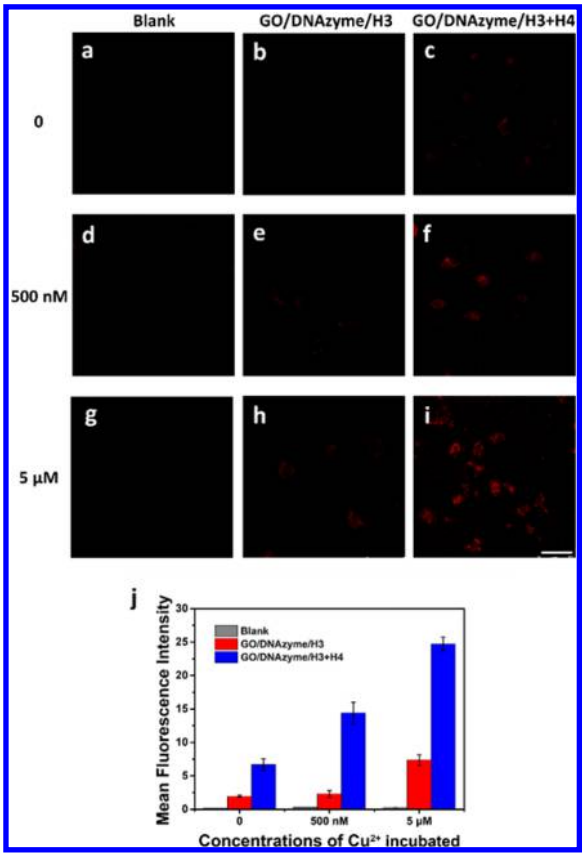

Figure 4. Fluorescence images (a–i) and quantitative analysis (j) of Cu^{2+} in MCF-7 cells using GO/DNAzyme/H3 + H4 sensors and GO/DNAzyme/H3 complex. Blank represents for cells without any sensors or complex added. The MCF-7 cells were incubated with Cu^{2+} solution of different concentrations (a–c, 0 nM; d–f, 500 nM; g, h, 5 μM). Scale bar is 50 μm.

The simultaneous detection of multiple metal ions can be an important means of studying the interactions and effects of metal ions. Next, we used the prepared sensors to perform the simultaneous in situ imaging of Zn^{2+} and Cu^{2+} in living cells. We labeled FAM on H1 and H2, which specifically respond to Zn^{2+}, allowing intracellular Zn^{2+} to be indicated by the green fluorescence of FAM. H3 and H4 are labeled with Cy5, which are specifically responsive to Cu^{2+}, thus, intracellular Cu^{2+} can be signaled by the red fluorescence of Cy5. MCF-7 cells were incubated for 1 h with 5 μM Zn^{2+} and 5 μM Cu^{2+}. Then, the resultant MCF-7 cells were incubated with GO/DNAzyme/H1 + H2 sensors and GO/DNAzyme/H3 + H4 sensors, followed by confocal imaging. As shown in Figure 5, the green fluorescence of FAM representing Zn^{2+} and the red fluorescence of Cy5 representing Cu^{2+} can be detected in different detection channels, which shows that our method can achieve the simultaneous distinction of two types of metal ions in cells. In order to verify the response of the sensors to the concentration changes of metal ions, we varied the ratio of Zn^{2+} to Cu^{2+} upon incubating with cells and performed the simultaneous fluorescence imaging of Zn^{2+} to Cu^{2+}. The

DOI: 10.1021/acs.analchem.7b05268
Anal. Chem. 2018, 90, 8785–8792

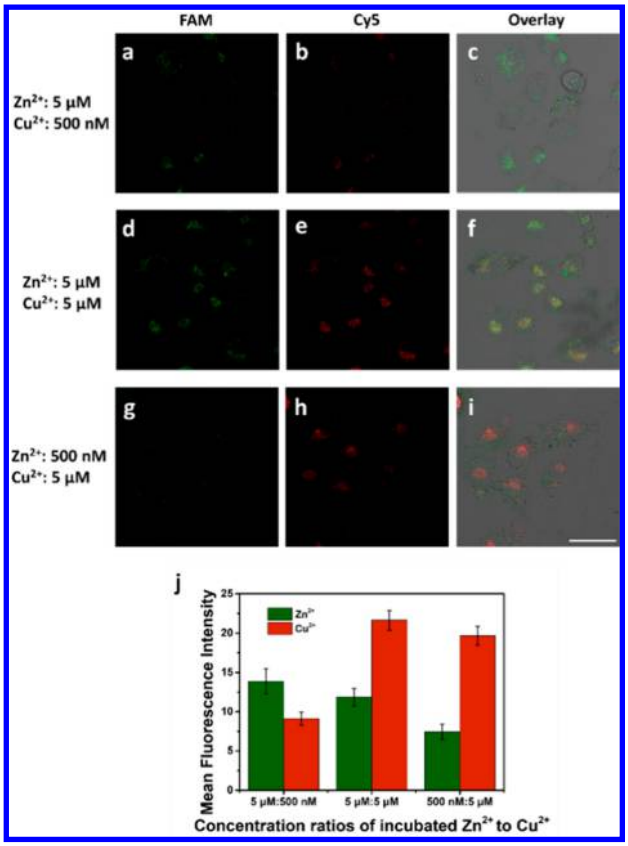

Figure 5. Fluorescence images (a–i) and quantitative analysis (j) of Zn^{2+} and Cu^{2+} in MCF-7 cells incubated with Zn^{2+} and Cu^{2+} mixtures with different concentration ratios of Zn to Cu^{2+} (concentration ratios of Zn^{2+} to Cu^{2+}: a–c, 500 nM:5 μM; d–f, 5 μM:5 μM; g, h, 5 μM:500 nM). FAM column represents the signal of Zn^{2+} and Cy5 column represents the signal of Cu^{2+}. Scale bar is 50 μm.

fluorescence of intracellular Zn^{2+} to Cu^{2+} were analyzed and semiquantitative data were obtained (Figure 5). With the varying ratio of Zn^{2+} to Cu^{2+} (5 μM:5 μM, 500 nM:5 μM, 5 μM:500 nM) upon incubating with cells, the intensity ratio of green fluorescence to red fluorescence representing the intracellular Zn^{2+} to Cu^{2+} changes correspondingly. The results illustrate the simultaneous fluorescence imaging can distinguish the individual changes of Zn^{2+} and Cu^{2+}.

CONCLUSIONS

In conclusion, to solve the problem of the simultaneous detection and in situ imaging of trace Zn^{2+} and Cu^{2+} in living cells, we developed a metal ion sensor with GO as a carrier, DNAzyme as a recognition unit for Zn^{2+} and Cu^{2+}, and DNA fragment and hairpin probe Hx as a signal transduction and amplification unit. Because of the enrichment of multiple fluorescent molecules caused by the DNA fragment-induced functional DNA self-assembly, the simultaneous imaging with high sensitivity of Zn^{2+} and Cu^{2+} in living cells can be achieved. The detection limits of the method for Zn^{2+} and Cu^{2+} were 100 and 80 pM, respectively, which were nearly 2 orders of magnitude higher than those of the previous best organic fluorescence probe. The results of this study are important for understanding the effects of low concentrations of Zn^{2+} and Cu^{2+} on cell function and the development of disease. Meanwhile, this work provides a new method for the simultaneous detection and in situ imaging of intracellular trace metal ions with high sensitivity.

ASSOCIATED CONTENT

Supporting Information

The Supporting Information is available free of charge on the ACS Publications website at DOI: 10.1021/acs.analchem.7b05268.

Sequences of oligonucleotides; Comparison of analytical performances; Optimization of GO concentration and time; Specificity evaluation of the sensors; Characterization of reaction kinetics; Evaluation of the stability; MTT assay of MCF-7 cells (PDF).

AUTHOR INFORMATION

Corresponding Authors

*E-mail: tangb@sdnu.edu.cn.

*E-mail: lilu5252@163.com. Fax: 86-531-86180017.

ORCID

Bo Tang: 0000-0002-8712-7025

Notes

The authors declare no competing financial interest.

ACKNOWLEDGMENTS

This work was supported by the National Natural Science Foundation of China (21535004, 91753111, 21390411, 21675104, and 21675102), the Natural Science Foundation of Shandong Province of China (ZR2016JL008, ZR2016BM02), and China Postdoctoral Science Foundation (2016M602179, 2017T100510).

REFERENCES

(1) Nies, D. H. *Appl. Microbiol. Biotechnol.* **1999**, *51*, 730–750.
(2) Carol, P.; Sreejith, S.; Ajayaghosh, A. *Chem. - Asian J.* **2007**, *2*, 338–348.
(3) Maret, W. *Adv. Nutr.* **2013**, *4*, 82–91.
(4) Vallee, B. L.; Falchuk, K. H. *Physiol. Rev.* **1993**, *73*, 79–118.
(5) Ra, H.-J.; Parks, W. C. *Matrix Biol.* **2007**, *26*, 587–596.
(6) Grabrucker, A.; Rowan, M.; Garner, C. *Drug Delivery Lett.* **2011**, *1*, 13–23.
(7) Zietz, B. P.; Dieter, H. H.; Lakomek, M.; Schneider, H.; Keßler-Gaedtke, B.; Dunkelberg, H. *Sci. Total Environ.* **2003**, *302*, 127–144.
(8) Georgopoulos, G. *J. Toxicol. Environ. Health, Part B* **2001**, *4*, 341–394.
(9) Brown, D. R.; Kozlowski, H. *Dalton Trans.* **2004**, 1907–1917.
(10) Vulpe, C.; Levinson, B.; Whitney, S.; Packman, S.; Gitschier, J. *Nat. Genet.* **1993**, *3*, 7–13.
(11) Waggoner, D. J.; Bartnikas, T. B.; Gitlin, J. D. *Neurobiol. Dis.* **1999**, *6*, 221–230.
(12) Viles, J. H. *Coord. Chem. Rev.* **2012**, *256*, 2271–2284.
(13) Şengör, S. S.; Gikas, P.; Moberly, J. G.; Peyton, B. M.; Ginn, T. R. *J. Chem. Technol. Biotechnol.* **2012**, *87*, 374–380.
(14) Lin, T.-W.; Huang, S.-D. *Anal. Chem.* **2001**, *73*, 4319–4325.
(15) Gonzáles, A. P. S.; Firmino, M. A.; Nomura, C. S.; Rocha, F. R. P.; Oliveira, P. V.; Gaubeur, I. *Anal. Chim. Acta* **2009**, *636*, 198–204.
(16) Pourreza, N.; Hoveizavi, R. *Anal. Chim. Acta* **2005**, *549*, 124–128.
(17) Ghaedi, M.; Niknam, K.; Taheri, K.; Hossainian, H.; Soylak, M. *Food Chem. Toxicol.* **2010**, *48*, 891–897.
(18) Liu, Y.; Liang, P.; Guo, L. *Talanta* **2005**, *68*, 25–30.
(19) Yang, L.; Hu, B.; Jiang, Z.; Pan, H. *Microchim. Acta* **2004**, *144*, 227–231.
(20) Karami, H.; Mousavi, M. F.; Yamini, Y.; Shamsipur, M. *Anal. Chim. Acta* **2004**, *509*, 89–94.

DOI: 10.1021/acs.analchem.7b05268
Anal. Chem. 2018, 90, 8785–8792

(21) Ramesh, A.; Devi, B. A.; Hasegawa, H.; Maki, T.; Ueda, K. *Microchem. J.* **2007**, *86*, 124−130.
(22) Wu, J.; Boyle, E. A. *Anal. Chem.* **1997**, *69*, 2464−2470.
(23) Becker, J. S.; Zoriy, M. V.; Pickhardt, C.; Palomero-Gallagher, N.; Zilles, K. *Anal. Chem.* **2005**, *77*, 3208−3216.
(24) Becker, J. S.; Matusch, A.; Depboylu, C.; Dobrowolska, J.; Zoriy, M. *Anal. Chem.* **2007**, *79*, 6074−6080.
(25) Anbu, S.; Ravishankaran, R.; Guedes da Silva, M. F. C.; Karande, A. A.; Pombeiro, A. J. L. *Inorg. Chem.* **2014**, *53*, 6655−6664.
(26) Jung, H. S.; Kwon, P. S.; Lee, J. W.; Kim, J. I.; Hong, C. S.; Kim, J. W.; Yan, S.; Lee, J. Y.; Lee, J. H.; Joo, T. *J. Am. Chem. Soc.* **2009**, *131*, 2008−2012.
(27) Zong, C.; Ai, K.; Zhang, G.; Li, H.; Lu, L. *Anal. Chem.* **2011**, *83*, 3126−3132.
(28) Wu, W.; Chen, A.; Tong, L.; Qing, Z.; Langone, K. P.; Bernier, W. E.; Jones, W. E. *ACS Sens.* **2017**, *2*, 1337−1344.
(29) Ding, Y.; Li, X.; Li, T.; Zhu, W.; Xie, Y. *J. Org. Chem.* **2013**, *78*, 5328−5338.
(30) Liu, X.; Zhang, N.; Zhou, J.; Chang, T.; Fang, C.; Shangguan, D. *Analyst* **2013**, *138*, 901−906.
(31) Huang, P.; Wu, F.; Mao, L. *Anal. Chem.* **2015**, *87*, 6834−6841.
(32) Rae, T. D.; Schmidt, P. J.; Pufahl, R. A.; Culotta, V. C.; O'Halloran, T. *Science* **1999**, *284*, 805−808.
(33) Chabosseau, P.; Tuncay, E.; Meur, G.; Bellomo, E. A.; Hessels, A.; Hughes, S.; Johnson, P. R. V.; Bugliani, M.; Marchetti, P.; Turan, B.; Lyon, A. R.; Merkx, M.; Rutter, G. A. *ACS Chem. Biol.* **2014**, *9*, 2111−2120.
(34) Zhang, X.-B.; Kong, R.-M.; Lu, Y. *Annu. Rev. Anal. Chem.* **2011**, *4*, 105−128.
(35) Hollenstein, M.; Hipolito, C.; Lam, C.; Dietrich, D.; Perrin, D. M. *Angew. Chem., Int. Ed.* **2008**, *47*, 4346−4350.
(36) Wen, Y.; Peng, C.; Li, D.; Zhuo, L.; He, S.; Wang, L.; Huang, Q.; Xu, Q. H.; Fan, C. *Chem. Commun.* **2011**, *47*, 6278−6280.
(37) Hollenstein, M.; Hipolito, C.; Lam, C.; Dietrich, D.; Perrin, D. M. *Angew. Chem., Int. Ed.* **2008**, *47*, 4346−4350.
(38) Lan, T.; Furuya, K.; Lu, Y. *Chem. Commun.* **2010**, *46*, 3896.
(39) Liu, J.; Brown, A. K.; Meng, X.; Cropek, D. M.; Istok, J. D.; Watson, D. B.; Lu, Y. *Proc. Natl. Acad. Sci. U. S. A.* **2007**, *104*, 2056−2061.
(40) Wu, P.; Hwang, K.; Lan, T.; Lu, Y. *J. Am. Chem. Soc.* **2013**, *135*, 5254−5257.
(41) Hwang, K.; Wu, P.; Kim, T.; Lei, L.; Tian, S.; Wang, Y.; Lu, Y. *Angew. Chem., Int. Ed.* **2014**, *53*, 13798−13802.
(42) Torabi, S. F.; Wu, P.; McGhee, C. E.; Chen, L.; Hwang, K.; Zheng, N.; Cheng, J.; Lu, Y. *Proc. Natl. Acad. Sci. U. S. A.* **2015**, *112*, 5903−5908.
(43) Wang, W.; Satyavolu, N. S. R.; Wu, Z.; Zhang, J. R.; Zhu, J. J.; Lu, Y. *Angew. Chem., Int. Ed.* **2017**, *56*, 6798−6802.
(44) Li, L.; Feng, J.; Fan, Y.; Tang, B. *Anal. Chem.* **2015**, *87*, 4829−4835.
(45) Wu, Z.; Fan, H.; Satyavolu, N. S. R.; Wang, W.; Lake, R.; Jiang, J. H.; Lu, Y. *Angew. Chem., Int. Ed.* **2017**, *56*, 8721−8725.
(46) Dirks, R. M.; Pierce, N. A. *Proc. Natl. Acad. Sci. U. S. A.* **2004**, *101*, 15275−15278.
(47) Xuan, F.; Hsing, I. M. *J. Am. Chem. Soc.* **2014**, *136*, 9810−9813.
(48) Ge, Z.; Lin, M.; Wang, P.; Pei, H.; Yan, J.; Shi, J.; Huang, Q.; He, D.; Fan, C.; Zuo, X. *Anal. Chem.* **2014**, *86*, 2124−2130.
(49) Peng, K.; Zhao, H.; Yuan, Y.; Yuan, R.; Wu, X. *Biosens. Bioelectron.* **2014**, *55*, 366−371.
(50) Yang, B.; Zhang, X.-B.; Kang, L.-P.; Shen, G.-L.; Yu, R.-Q.; Tan, W. *Anal. Chem.* **2013**, *85*, 11518−11523.
(51) Li, L.; Feng, J.; Liu, H.; Li, Q.; Tong, L.; Tang, B. *Chem. Sci.* **2016**, *7*, 1940−194.
(52) Zhao, X.-H.; Kong, R.-M.; Zhang, X.-B.; Meng, H.-M.; Liu, W.-N.; Tan, W.; Shen, G.-L.; Yu, R.-Q. *Anal. Chem.* **2011**, *83*, 5062−5066.
(53) Freeman, R.; Liu, X.; Willner, I. *J. Am. Chem. Soc.* **2011**, *133*, 11597−11604.
(54) Wu, C.-S.; Khaing Oo, M. K.; Fan, X. *ACS Nano* **2010**, *4*, 5897−5904.
(55) Liu, S.; Na, W.; Pang, S.; Su, X. *Biosens. Bioelectron.* **2014**, *58*, 17−21.
(56) Yao, J.; Li, J.; Owens, J.; Zhong, W. *Analyst* **2011**, *136*, 764−768.
(57) Wang, H.-B.; Wang, L.; Huang, K.-J.; Xu, S.-P.; Wang, H.-Q.; Wang, L.-L.; Liu, Y.-M. *New J. Chem.* **2013**, *37*, 2557−2563.
(58) Liu, J.; Lu, Y. *J. Am. Chem. Soc.* **2003**, *125*, 6642−6643.
(59) Liu, J.; Lu, Y. *J. Am. Chem. Soc.* **2004**, *126*, 12298−12305.
(60) Luo, Y.; Zhang, Y.; Xu, L.; Wang, L.; Wen, G.; Liang, A.; Jiang, Z. *Analyst* **2012**, *137*, 1866−1871.
(61) Xiang, Y.; Lu, Y. *Chem. Commun.* **2013**, *49*, 585−587.
(62) Liu, Z.; Robinson, J. T.; Sun, X.; Dai, H. *J. Am. Chem. Soc.* **2008**, *130*, 10876−10877.
(63) Mohanty, N.; Berry, V. *Nano Lett.* **2008**, *8*, 4469−4476.
(64) Li, J.; Zheng, W.; Kwon, A. H.; Lu, Y. *Nucleic Acids Res.* **2000**, *28*, 481−488.
(65) Pyle, A. M. *Science* **1993**, *261*, 709−714.
(66) Liu, J.; Lu, Y. *J. Am. Chem. Soc.* **2007**, *129*, 9838−9839.
(67) Elbaz, J.; Shlyahovsky, B.; Willner, I. *Chem. Commun.* **2008**, 1569−1571.
(68) Lu, C. H.; Yang, H. H.; Zhu, C. L.; Chen, X.; Chen, G. N. *Angew. Chem.* **2009**, *121*, 4879−4881.
(69) Wen, Y.; Peng, C.; Li, D.; Zhuo, L.; He, S.; Wang, L.; Huang, Q.; Xu, Q.-H.; Fan, C. *Chem. Commun.* **2011**, *47*, 6278−6280.
(70) He, S.; Song, B.; Li, D.; Zhu, C.; Qi, W.; Wen, Y.; Wang, L.; Song, S.; Fang, H.; Fan, C. *Adv. Funct. Mater.* **2010**, *20*, 453−459.
(71) Zhang, Z.; Balogh, D.; Wang, F.; Willner, I. *J. Am. Chem. Soc.* **2013**, *135*, 1934−1940.
(72) Liu, H.; Li, L.; Wang, Q.; Duan, L.; Tang, B. *Anal. Chem.* **2014**, *86*, 5487−5493.
(73) Tang, Z.; Wu, H.; Cort, J. R.; Buchko, G. W.; Zhang, Y.; Shao, Y.; Aksay, I. A.; Liu, J.; Lin, Y. *Small* **2010**, *6*, 1205−1209.
(74) Hu, X.; Mu, L.; Wen, J.; Zhou, Q. *J. Hazard. Mater.* **2012**, *213*, 387−392.

DOI: 10.1021/acs.analchem.7b05268
Anal. Chem. 2018, 90, 8785−8792